Electronic Supplementary Material (ESI) for Physical Chemistry Chemical Physics.

Supporting information for

Concerted Double Proton-Transfer Electron-Transfer between Catechol and Superoxide Radical Anion

Jorge Quintero-Saumeth[a,b], *David A., Rincón*[a,c], *Markus Doerr*[b], *Martha C. Daza*[b]

[a] *Grupo de Bioquímica Teórica, Universidad Industrial de Santander, Bucaramanga, Colombia.*
[b] *Universidad de Pamplona, Facultad de Ciencias Básicas, Pamplona, Colombia*
[c] *Facultad de Ingeniería, Pontificia Universidad Javeriana, Bogotá, Colombia.*

S1. Thermochemistry of the reaction mechanisms between catechol and superoxide radical anion

Five reaction mechanisms between catechol and the superoxide anion radical were thermochemically analyzed.

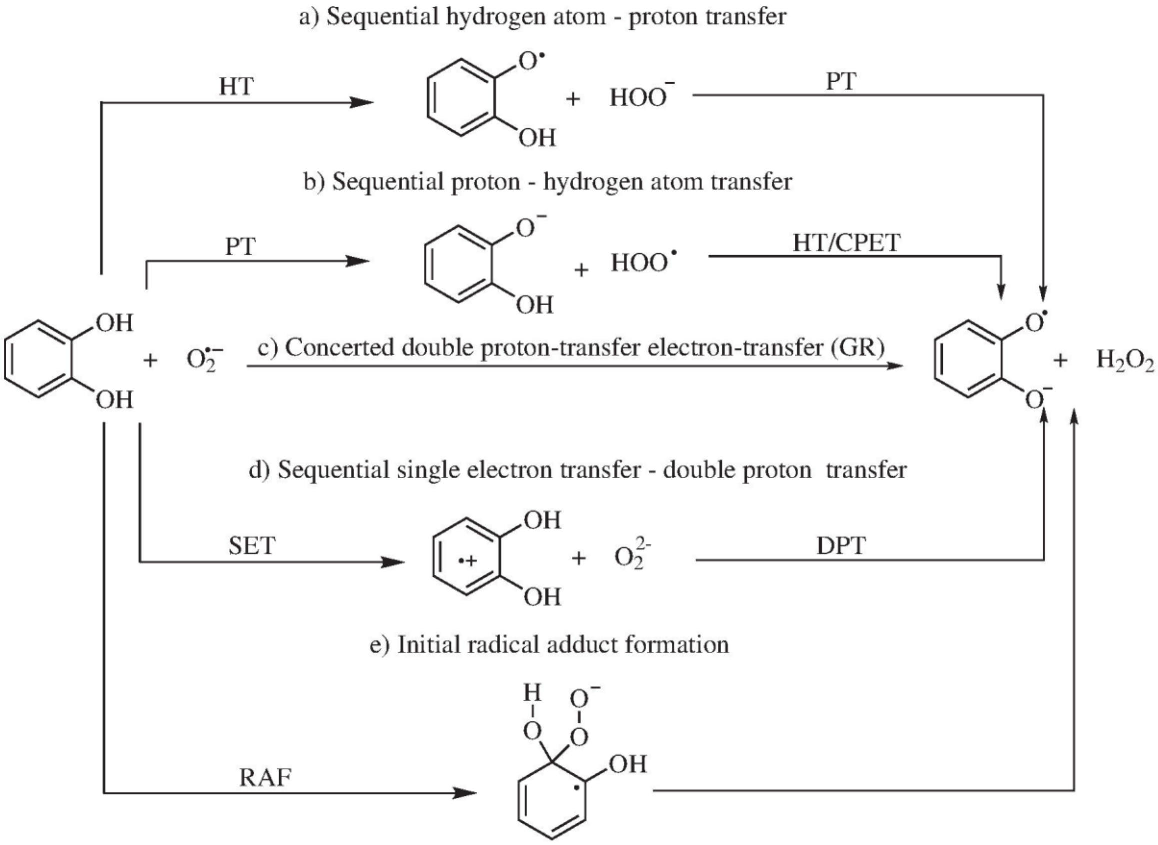

Figure S1. Possible mechanisms of reaction between catechol and superoxide anion radical to produce catecholate anion radical and hydrogen peroxide.[1–5]

1. <u>Mechanism I (HT-PT):</u> This mechanism consists of two steps: i) initial transfer of a hydrogen atom from catechol to the superoxide radical anion yielding hydroperoxide anion and catechol radical (HT). ii) Transfer of a proton from catechol radical to hydroperoxide anion yielding hydrogen peroxide and catecholate anion radical (PT). (See Fig. S2).

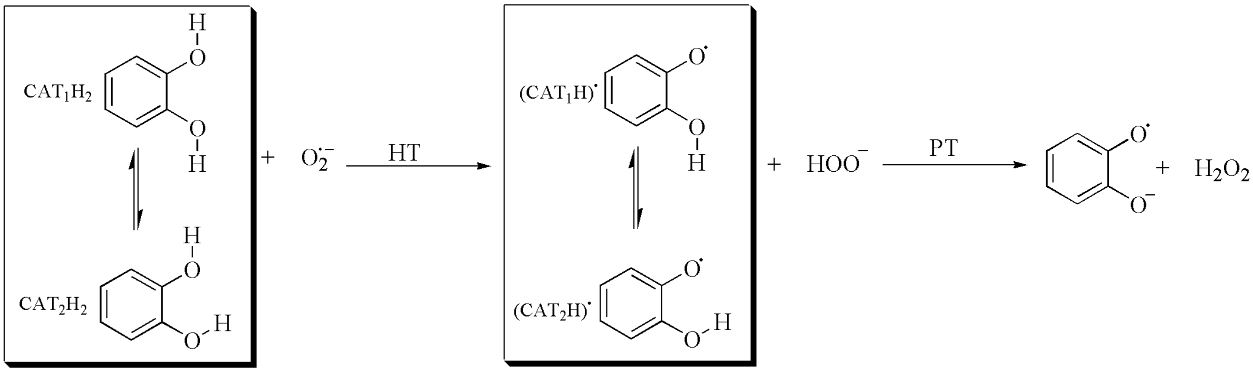

Figure S2. Schematic representation of the HT-PT reaction mechanism. Step 1 = initial hydrogen atom transfer (HT) from catechol to superoxide radical anion. Step 2 = proton transfer from the catechol radical conformers $(\mathrm{CAT_1H})^\bullet$ and $(\mathrm{CAT_2H})^\bullet$ to hydroperoxide anion.

The free energy change in water, DMF and PEA solvents for the first step of the mechanism HT-PT was calculated using the following equation:

$$\Delta G^{\mathrm{HT}}_{\mathrm{sol.}} = \left[G^{\mathrm{HOO^-}}_{\mathrm{sol.}} + \sum\nolimits_n f_i \cdot G^{(\mathrm{CAT_iH})^\bullet}_{\mathrm{sol.}}\right] - \left[G^{\mathrm{O_2^{\bullet-}}}_{\mathrm{sol.}} + \sum\nolimits_n f_i \cdot G^{\mathrm{CAT_iH_2}}_{\mathrm{sol.}}\right] \qquad \text{(S1)}$$

$G^{\mathrm{HOO^-}}_{\mathrm{sol.}}$, $G^{(\mathrm{CAT_iH})^\bullet}_{\mathrm{sol.}}$, $G^{\mathrm{O_2^{\bullet-}}}_{\mathrm{sol.}}$ and $G^{\mathrm{CAT_iH_2}}_{\mathrm{sol.}}$ are the free energies of the hydroperoxide anion, the *ith* catechol radical conformer (only two conformers), superoxide radical anion and the *ith* catechol conformer (only two conformers) in solution. The free energy in solution for each molecule is calculated using

$$G^{\mathrm{(i)}}_{\mathrm{sol.}} = G^{\mathrm{(i)}}_{\mathrm{gas}} + \Delta G_{\mathrm{solv}} + \Delta G_{1\ \mathrm{atm}\to 1\ \mathrm{M}} \qquad \text{(S2)}$$

where $G^{\mathrm{(i)}}_{\mathrm{gas}}$, ΔG_{solv} and $\Delta G_{1\ \mathrm{atm}\to 1\ \mathrm{M}}$ are the free energies in the gas phase, the energy of solvation (single point energy calculation using the geometry optimized in gas phase). The final expression corresponds to an additional term to convert 1 atm pressure (gas phase) to 1 mol $\mathrm{L^{-1}}$ (solution), which is equivalent to 7.91 kJ $\mathrm{mol^{-1}}$.[6] The other term in equation S1 is f_i, which is the population of the *ith* neutral and anionic conformer of catechol. It is calculated by applying a Boltzmann statistics expression:

$$f_i = \frac{\exp\left(-\frac{G_{\text{sol.}}^{(\text{i})}}{RT}\right)}{\sum_n \exp\left(-\frac{G_{\text{sol.}}^{(\text{i})}}{RT}\right)} \qquad \text{(S3)}$$

where *R* is the ideal gas constants and *T* is the absolute temperature.

On the other hand, the free energy change in gas phase was calculated using similar mathematical expressions as those presented in equations S1-S3, but using only the free energy in gas phase, which is calculated using equation S4:

$$G_{\text{gas}}^{(\text{i})} = E_o^{\text{DFT or CCSD(T)/CBS}} + \mathrm{G}_{\text{corr}}^{\text{DFT}} \qquad \text{(S4)}$$

where $E_o^{\text{DFT or CCSD(T)/CBS}}$ is the electronic energy calculated either at the DFT (using B3LYP or M06-2X with the 6-311+G(3df,2p) basis set) or CCSD(T)/CBS level. $\mathrm{G}_{\text{corr}}^{\text{DFT}}$ is the correction of the electronic energy to obtain the gas phase free energy at the B3LYP/6-311+G(3df,2p) or M06-2X/6-311+G(3df,2p) optimized geometry in vacuum at standard conditions (G°, T = 298.15 K, P = 1 atm).

The free energy change of the second stage of the HT-PT mechanism in solution was calculated from equation S5:

$$\Delta G_{\text{sol.}}^{\text{PT}} = \left[G_{\text{sol.}}^{\text{H}_2\text{O}_2} + G_{\text{sol.}}^{(\text{CAT})^{\bullet -}}\right] - \left[G_{\text{sol.}}^{\text{HOO}^-} + \sum_n f_i \cdot G_{\text{sol.}}^{(\text{CAT}_\text{i}\text{H})^{\bullet}}\right] \qquad \text{(S5)}$$

$G_{\text{sol.}}^{\text{H}_2\text{O}_2}$, $G_{\text{sol.}}^{(\text{CAT})^{\bullet -}}$, $G_{\text{sol.}}^{\text{HOO}^-}$ and $G_{\text{sol.}}^{(\text{CAT}_\text{i}\text{H})^{\bullet}}$ are the free energies of hydrogen peroxide, the catecholate anion radical, the hydroperoxide anion and the *ith* catechol radical conformer (only two conformers) in solution calculated from equation S2, f_i is the population of the *ith* catechol radical conformer (only two conformers) using equation S3. For the same stage of mechanism HT-PT, the free energy change in gas phase was calculated using only the free energy in gas phase (using equation S4):

$$\Delta G_{\text{gas}}^{\text{PT}} = \left[G_{\text{gas}}^{\text{H}_2\text{O}_2} + G_{\text{gas}}^{(\text{CAT})^{\bullet -}}\right] - \left[G_{\text{gas}}^{\text{HOO}^-} + \sum_n f_i \cdot G_{\text{gas}}^{(\text{CAT}_\text{i}\text{H})^{\bullet}}\right] \qquad \text{(S6)}$$

2. Mechanism II (PT-HT): This mechanism consists of two stages: i) initial transfer of a proton from catechol to the superoxide anion radical, forming catecholate anion and perhydroxyl radical (PT). ii) transfer of a hydrogen atom from the catecholate anion to perhydroxyl radical, finally yielding catecholate anion radical and hydrogen peroxide. (See Fig. S3)

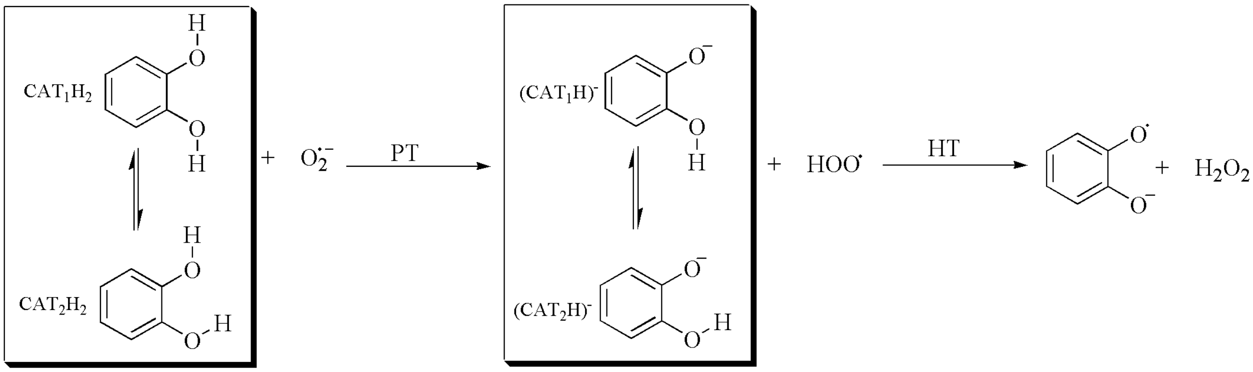

Figure S3. Schematic representation of the PT-HT reaction mechanism. Step 1 = initial proton transfer (PT) from catechol to superoxide radical anion. Step 2 = hydrogen atom transfer (HT) from the catecholate anion conformers $(CAT_1H)^-$ and $(CAT_2H)^-$ to perhydroxyl radical.

The free energy change in the first step of the PT-HT mechanism in solution was calculated from equation S7:

$$\Delta G_{\text{sol.}}^{\text{PT}} = \left[G_{\text{sol.}}^{\text{HOO}^\bullet} + \sum\nolimits_n f_i \cdot G_{\text{sol.}}^{(\text{CAT}_i\text{H}_1)^-} \right] - \left[G_{\text{sol.}}^{\text{O}_2^{\bullet-}} + \sum\nolimits_n f_i \cdot G_{\text{sol.}}^{\text{CAT}_i\text{H}_2} \right] \qquad \text{(S7)}$$

where $G_{\text{sol.}}^{\text{HOO}^\bullet}$, $G_{\text{sol.}}^{(\text{CAT}_i\text{H}_1)^-}$, $G_{\text{sol.}}^{\text{O}_2^{\bullet-}}$ and $G_{\text{sol.}}^{\text{CAT}_i\text{H}_2}$ are the free energies of the perhydroxyl radical, the *ith* catecholate anion conformer (only two conformers), the superoxide radical anion and the *ith* catechol conformer (only two conformers) in solution, calculated from equation S2. f_i is the population of the *ith* catecholate anion and catechol conformer calculated from equation S3. For the same stage of the PT-HT mechanism the free energy change in gas phase was calculated using only the free energy in gas phase (using the equation S4):

$$\Delta G_{\text{gas}}^{\text{PT}} = \left[G_{\text{gas}}^{\text{HOO}^\bullet} + \sum\nolimits_n f_i \cdot G_{\text{gas}}^{(\text{CAT}_i\text{H}_1)^-} \right] - \left[G_{\text{gas}}^{\text{O}_2^{\bullet-}} + \sum\nolimits_n f_i \cdot G_{\text{gas}}^{\text{CAT}_i\text{H}_2} \right] \text{(S8)}$$

The free energy change of the second stage of the mechanism PT-HT in solution was calculated from the following equation

$$\Delta G_{\text{sol.}}^{\text{HT}} = \left[G_{\text{sol.}}^{\text{H}_2\text{O}_2} + G_{\text{sol.}}^{(\text{CAT})^{\bullet-}} \right] - \left[G_{\text{sol.}}^{\text{HOO}^\bullet} + \sum\nolimits_n f_i \cdot G_{\text{sol.}}^{(\text{CAT}_i\text{H})^-} \right] \qquad \text{(S9)}$$

$G_{\text{sol.}}^{\text{H}_2\text{O}_2}$, $G_{\text{sol.}}^{(\text{CAT})^{\bullet-}}$, $G_{\text{sol.}}^{\text{HOO}^\bullet}$ and $G_{\text{sol.}}^{(\text{CAT}_i\text{H})^-}$ are the free energies of hydrogen peroxide, the catecholate anion radical, the perhydroxyl and the *ith* catecholate anion conformer (only two conformers) in solution phase calculated from equation S2. f_i is the population of the *ith* catecholate anion conformer (only two conformers) using equation S3. For the same stage of the HT-PT mechanism the free energy change in gas phase was calculated using only the free energy in gas phase (using equation S4) by:

$$\Delta G_{\text{gas}}^{\text{HT}} = \left[G_{\text{gas}}^{\text{H}_2\text{O}_2} + G_{\text{gas}}^{(\text{CAT})^{\bullet-}} \right] - \left[G_{\text{gas}}^{\text{HOO}^\bullet} + \sum\nolimits_n f_i \cdot G_{\text{gas}}^{(\text{CAT}_i\text{H})^-} \right] \qquad \text{(S10)}$$

3. <u>Mechanism III (GR):</u> This corresponds to the transfer of a proton and a hydrogen atom from catechol to the superoxide radical anion producing catecholate anion radical and hydrogen peroxide in the absence of intermediates (see Fig. S4).

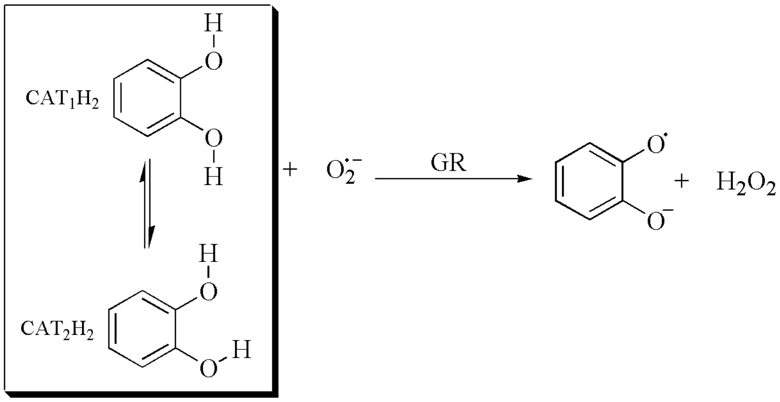

Figure S4. Schematic representation of the simultaneous proton – hydrogen atom transfer (called GR).

The free energy change of mechanism GR in solution was calculated from the following equation:

$$\Delta G_{\text{sol.}}^{\text{GR}} = \left[G_{\text{sol.}}^{\text{H}_2\text{O}_2} + G_{\text{sol.}}^{(\text{CAT})^{\bullet-}} \right] - \left[G_{\text{sol.}}^{\text{O}_2^{\bullet-}} + \sum\nolimits_n f_i \cdot G_{\text{sol.}}^{\text{CAT}_i\text{H}_2} \right] \qquad \text{(S11)}$$

where $G^{H_2O_2}_{sol.}$, $G^{(CAT)^{\bullet-}}_{sol.}$, $G^{O_2^{\bullet-}}_{sol.}$ and $G^{CAT_iH_2}_{sol.}$ are the free energies of hydrogen peroxide, catecholate anion radical, the superoxide radical anion and the *ith* catechol conformer (only two conformers) in solution, calculated from equation S2. f_i is the population of the *ith* catechol conformer calculated from equation S3. For the same stage of the PT-HT mechanism the free energy change in gas phase was calculated using only the free energy in gas phase (using the equation S4) using

$$\Delta G^{GR}_{gas} = \left[G^{H_2O_2}_{gas} + G^{(CAT)^{\bullet-}}_{gas}\right] - \left[G^{O_2^{\bullet-}}_{gas} + \sum\nolimits_n f_i \cdot G^{CAT_iH_2}_{gas}\right] \quad (S12)$$

4. <u>Mechanism IV (SET-DPT):</u> This mechanism starts with the transfer of an electron from catechol to the superoxide anion radical, producing molecular oxygen dianion and catechol cation radical. Subsequently, two protons are transferred from the catechol cation radical to molecular oxygen dianion to produce catecholate anion radical and hydrogen peroxide. This mechanism can be analyzed using the redox potentials of each half reaction. (See Fig. S5).

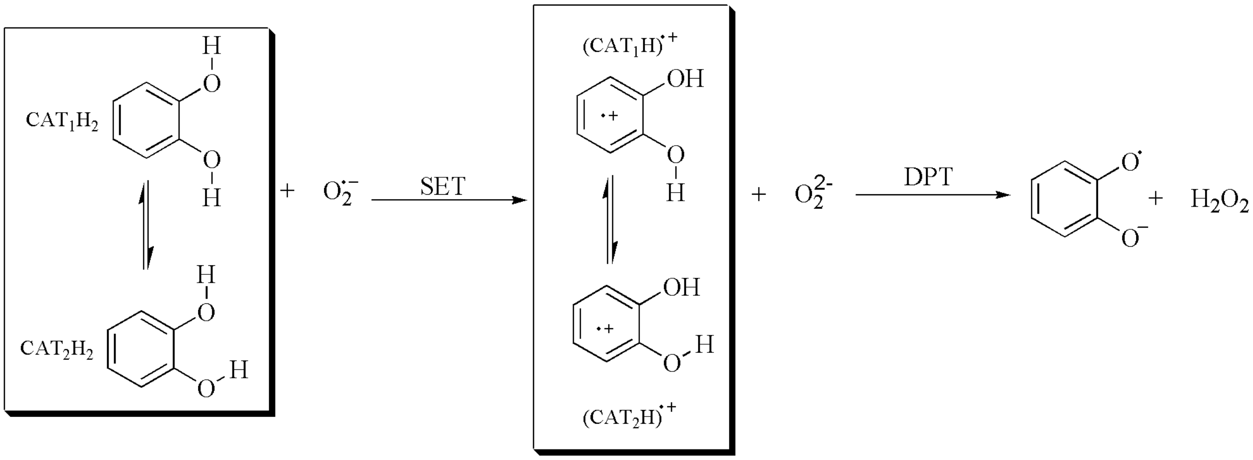

Figure S5. Schematic representation of the SET-DPT reaction mechanism. Step 1 = initial single electron (SET) from catechol to superoxide radical anion. Step 2 = double proton transfer (DPT) from the catechol cation radical conformers $(CAT_1H)^{\bullet+}$ and $(CAT_2H)^{\bullet+}$ to molecular oxygen dianion.

The free energy change of the first step of the mechanism SET-DPT in solution was calculated from equation

$$\Delta G^{\mathrm{SET}}_{\mathrm{sol.}} = \left[G^{\mathrm{O}_2^{2-}}_{\mathrm{sol.}} + \sum\nolimits_n f_i \cdot G^{(\mathrm{CAT_iH_2})^{\bullet+}}_{\mathrm{sol.}} \right] - \left[G^{\mathrm{O}_2^{\bullet-}}_{\mathrm{sol.}} + \sum\nolimits_n f_i \cdot G^{\mathrm{CAT_iH_2}}_{\mathrm{sol.}} \right] \qquad \text{(S13)}$$

Where $G^{\mathrm{O}_2^{2-}}_{\mathrm{sol.}}$, $G^{(\mathrm{CAT_iH_2})^{\bullet+}}_{\mathrm{sol.}}$, $G^{\mathrm{O}_2^{\bullet-}}_{\mathrm{sol.}}$ and $G^{\mathrm{CAT_iH_2}}_{\mathrm{sol.}}$ are the free energies of the molecular oxygen dianion, the *ith* catechol cation radical (only two conformers), the superoxide radical anion and the *ith* catechol conformer (only two conformers) in solution, calculated from equation S2. f_i is the population of the *ith* catechol cation radical and catechol calculated from equation S3. For the same stage of the SET-DPT mechanism the free energy change in gas phase was calculated using only the free energy in gas phase (using equation S4):

$$\Delta G^{\mathrm{SET}}_{\mathrm{gas}} = \left[G^{\mathrm{O}_2^{2-}}_{\mathrm{gas}} + \sum\nolimits_n f_i \cdot G^{(\mathrm{CAT_iH_2})^{\bullet+}}_{\mathrm{gas}} \right] - \left[G^{\mathrm{O}_2^{\bullet-}}_{\mathrm{gas}} + \sum\nolimits_n f_i \cdot G^{\mathrm{CAT_iH_2}}_{\mathrm{gas}} \right] \quad \text{(S14)}$$

The free energy change of the second step of the mechanism SET-DPT in solution phase was calculated from equation S15:

$$\Delta G^{\mathrm{DPT}}_{\mathrm{sol.}} = \left[G^{\mathrm{H_2O_2}}_{\mathrm{sol.}} + G^{(\mathrm{CAT})^{\bullet-}}_{\mathrm{sol.}} \right] - \left[G^{\mathrm{O}_2^{2-}}_{\mathrm{sol.}} + \sum\nolimits_n f_i \cdot G^{(\mathrm{CAT_iH_2})^{\bullet+}}_{\mathrm{sol.}} \right] \qquad \text{(S15)}$$

Where $G^{\mathrm{H_2O_2}}_{\mathrm{sol.}}$, $G^{(\mathrm{CAT})^{\bullet-}}_{\mathrm{sol.}}$, $G^{\mathrm{O}_2^{2-}}_{\mathrm{sol.}}$ and $G^{(\mathrm{CAT_iH_2})^{\bullet+}}_{\mathrm{sol.}}$ are the free energies of hydrogen peroxide, the catecholate anion radical, the molecular oxygen dianion and the *ith* catechol cation radical (only two conformers) in solution calculated from equation S2. f_i is the population of the *ith* catechol cation radical calculated from equation S3. For the same stage of the SET-DPT mechanism the free energy change in gas phase was calculated using only the free energy in gas phase (using equation S4):

$$\Delta G^{\mathrm{DPT}}_{\mathrm{gas}} = \left[G^{\mathrm{H_2O_2}}_{\mathrm{gas}} + G^{(\mathrm{CAT})^{\bullet-}}_{\mathrm{gas}} \right] - \left[G^{\mathrm{O}_2^{2-}}_{\mathrm{gas}} + \sum\nolimits_n f_i \cdot G^{(\mathrm{CAT_iH_2})^{\bullet+}}_{\mathrm{gas}} \right] \quad \text{(S16)}$$

S2. Electronic and structural analysis, M06-2X functional

In addition to the analysis with the B3LYP functional, which is described in the main text, we have performed this analysis using the M06-2X functional. The results are presented in this section.

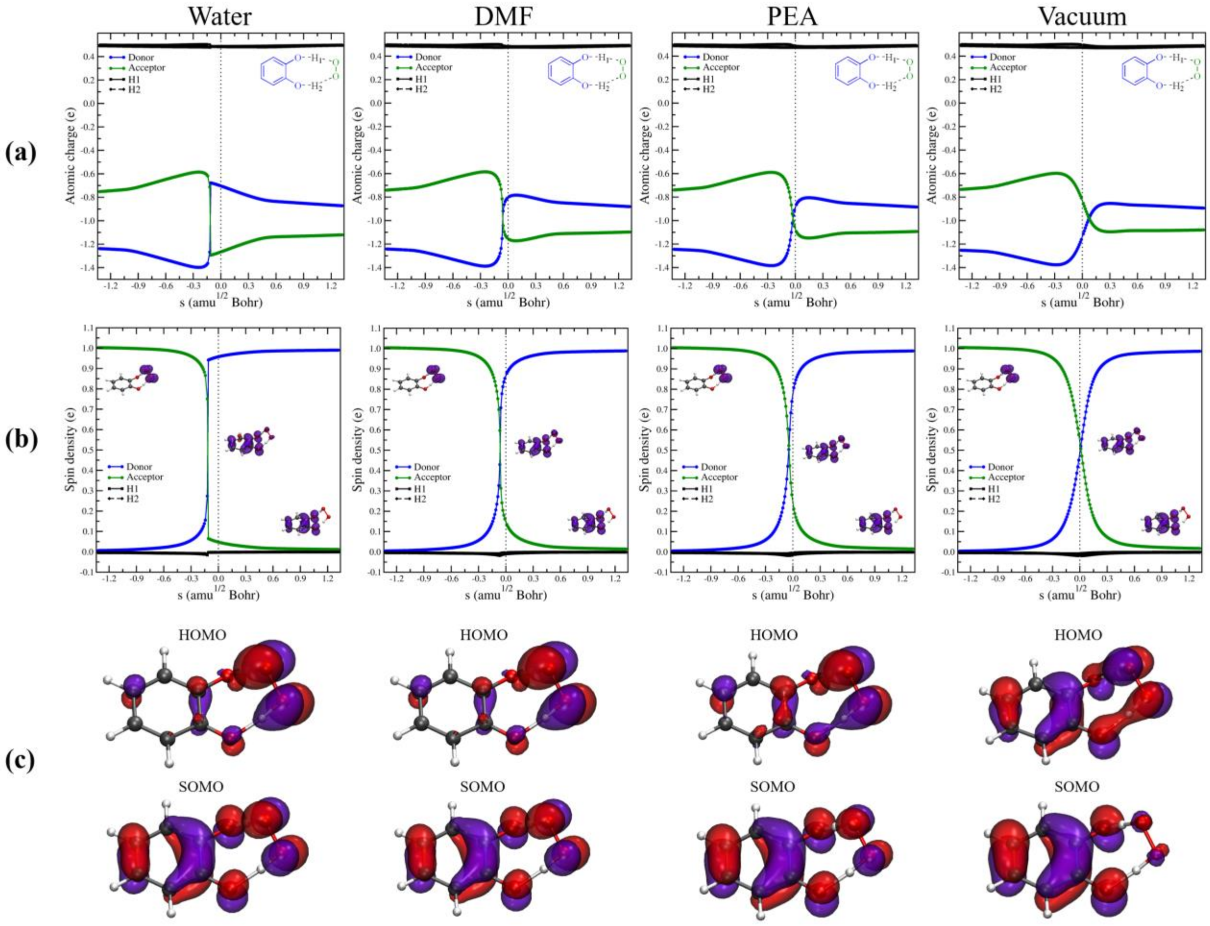

Figure S6. Natural population analysis and frontier molecular orbital analysis along the reaction coordinate for catechol and superoxide radical anion at the UM06-2X/6-311+G(3df,2p) level of theory in water, DMF, PEA and gas phase. (a) Atomic charge analysis, (b) atomic spin density (c) frontier molecular orbital analysis of catechol/superoxide in the gas phase at the structure of the TS. Donor: catechol moiety without H_1 and H_2 atoms. Acceptor: superoxide radical anion without H_1 and H_2 atoms. Negative values of s (amu$^{1/2}$ Bohr) represent the region connecting the TS with PRC and positive values of s (amu$^{1/2}$ Bohr) represent the region connecting TS with PC. Solvent effects were simulated using the SMD solvation model.

S3. Optimized structures of catechol, H_2O_2 and $HOO^{\bullet}$ and comparison with experimental data

In this section we present details of the optimized structures of catechol, hydrogen peroxide and perhydroxyl radical and a comparison with experimental data.

Table S1. Geometrical parameters for catechol, CAT_1H_2 conformer, at different levels of theory and experimental values (bond lengths in Å and valence angles in degrees).

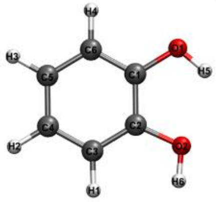

Bond length (Å)	Exp. 1[a]	Exp. 2[b]	B3LYP/6-311+G(3df,2p)	M06-2X/6-311+G(3df,2p)
C1-C2	1.4000	1.3900	1.4020	1.3960
C2-C3	1.3870	1.3810	1.3900	1.3820
C3-C4	1.4010	1.3840	1.3980	1.3910
C4-C5	1.3940	1.3860	1.3940	1.3850
C5-C6	1.4000	1.3850	1.3970	1.3890
C3-H1	1.0800	1.0000	1.0870	1.0840
C4-H2	1.0780	0.9600	1.0840	1.0810
C5-H3	1.0780	0.9800	1.0850	1.0810
C6-H4	1.0770	1.0100	1.0850	1.0820
C1-O1	1.3670	1.3640	1.3640	1.3550
C2-O2	1.3830	1.3730	1.3780	1.3680
O1-H5	0.9640	0.8000	0.9670	0.9630
O2-H6	0.9600	0.9100	0.9630	0.9590
Valence angle (°)	Exp. Value 1[a]	Exp. Value 2[b]	B3LYP/6-311+G(3df,2p)	M06-2X/6-311+G(3df,2p)
C1-C2-C3	120.9	119.7	120.4	120.5
C2-C3-C4	119.4	120.1	119.9	119.8
C3-C4-C5	119.4	120.1	119.8	119.8
C4-C5-C6	120.3	119.8	120.2	120.3
H1-C3-C4	120.5	123	120.5	120.7
H2-C4-C5	120.4	120	120.6	120.5
H3-C5-C6	119.6	119	119.5	119.6
H4-C6-C1	118.5	119	118.5	118.4
O1-C1-C2	120.8	121	120.7	120.4
O2-C2-C1	114.1	123	115.3	115.2
H5-O1-C1	106.4	111	108.6	108.7
H6-O2-C2	109.4	106	110.3	110.4
Dihedral angle (°)			B3LYP/6-311+G(3df,2p)	M06-2X/6-311+G(3df,2p)
C_2-C_1-O_1-H_5			0.0	0.0
C_1-C_2-O_2-H_6			180.0	180.0

[a] Reference 7.
[b] Reference 8.
[d] Calculated with the experimental value 1
[e] Calculated with the experimental value 2
[f] Calculated with the experimental value 1
[g] Calculated with the experimental value 2

Table S2. Geometrical parameters hydrogen peroxide and perhydroxyl radical at different levels of theory and experimental values (bond lengths in Å and valence angles in degrees).

		B3LYP 6-311+G(3df,2p)		M06-2X 6-311+G(3df,2p)	
Hydrogen peroxide (H_2O_2)					
Parameter	Exp. [a]	Calculated	Diff.	Calculated	Diff.
O1-O2	1.475	1.446	0.029	1.418	0.057
O1-H3	0.950	0.966	-0.016	0.963	-0.013
O2-H4	0.950	0.966	-0.016	0.963	-0.013
H3-O1-O2	94.8	100.9	-6.1	101.7	-6.9
H4-O1-O2	94.8	100.9	-6.1	101.7	-6.9
H3-O1-O2-H4	119.8	111.9	7.9	110.7	9.1
Perhydroxyl radical ($HOO^\bullet$)					
Parameter	Exp. [b]	Calculated	Diff.	Calculated	Diff.
O1-O2	1.331	1.324	0.007	1.304	0.027
O1-H1	0.971	0.975	-0.004	0.972	-0.001
H1-O1-O2	104.3	105.6	-1.3	105.9	-1.6

[a] Reference 9.

[b] Reference 10.

Table S3. Chemical parameters used for calculating the free energy changes in aqueous phase for the mechanisms HT-PH, HT-PT y GR.

Parameter	Experimental value	Reference
$E^o{}_1$ ($CATH^\bullet/CATH^-$): $CATH^\bullet + 1e^- \rightarrow CATH^-$	0.69	Ref. 11
$E^o{}_2$ ($CAT^{\cdot -}/CAT^{-2}$): $CAT^{\bullet -} + 1e^- \rightarrow CAT^{-2}$	0.20	Ref. 11
$E^o{}_1$ ($HOO^\cdot/HOO^-$): $HOO^\bullet + 1e^- \rightarrow HOO^-$	0.75	Ref. 11
pK_{a1}(catechol): $CATH_2 \rightarrow CATH^- + H^+$		
	9.30	Ref. 12
	9.45	Ref. 13
	9.40	Ref. 14
	9.26	Ref. 15
	9.25	Ref. 16
	9.50	Ref. 17
pK_{a2}(catechol): $CATH^- \rightarrow CAT^{-2} + H^+$		
	12.8	Ref. 13
	13.4	Ref. 15
	13.0	Ref. 16
pK_{a3}(catechol): $CATH^\bullet \rightarrow CAT^{\bullet -} + H^+$	5.0	Ref. 11
pK_{a1} $HOO^\bullet$): $HOO^\bullet \rightarrow O_2{}^{\bullet -} + H^+$		
	4.7	Ref. 18
	4.9	Ref. 19
pK_{a2} (H2O2): $H_2O_2 \rightarrow HOO^- + H^+$	11.6	Ref. 20
E^o ($CAT^{\bullet -}/CATH_2$): $CAT^{\bullet -} + 2H^+ + 1e^- \rightarrow CATH_2$		
	0.540	Ref. 21
	0.530	Ref. 13
E^o ($O_2{}^-/H_2O_2$): $O_2{}^- + 2H^+ + 1e^- \rightarrow H_2O_2$		
	0.940	Ref. 22
	0.890	Ref. 18
BDFE(catechol): $CATH_2 \rightarrow CATH_1{}^\bullet + H^\bullet$	361.2	Ref 11
BDFE(catechol anion): $CATH_1{}^- \rightarrow CAT^{\bullet -} + H^\bullet$	335.2	Ref 11
BDFE(HOO^-): $HOO^- \rightarrow O_2{}^- + H^\bullet$	340.8	Ref 11
BDFE(H_2O_2): $H_2O_2 \rightarrow HOO^\bullet + H^\bullet$	379.9	Ref 11

S4. Structures of the pre-reactive complexes, transition states and product complexes

Here we present structural parameters of the pre-reactive complexes, transition states and product complexes, obtained with the B3LYP and the M06-2X functional.

Table S4. Geometrical parameters for PRC, TS and PC of the concerted reaction mechanism between catechol and superoxide radical anion, obtained with the B3LYP and M06-2X functionals and the 6-311+G(3df,2p) basis set. Bond lengths (*d*) in Å. Valence and dihedral angles in degrees.

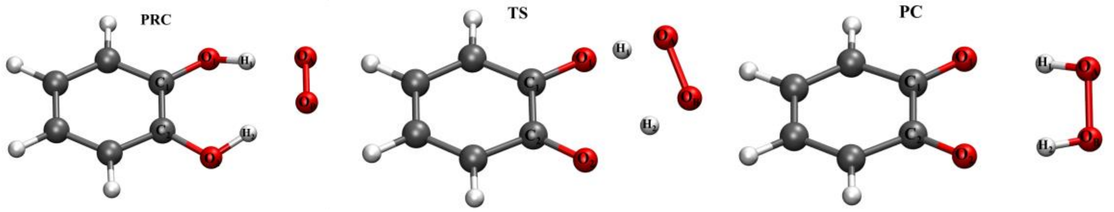

	B3LYP/6-311+G(3df,2p)			M06-2X/6-311+G(3df,2p)		
Geometrical parameter	PRC	TS	PC	PRC	TS	PC
d(C$_1$-C$_2$)	1.4215	1.4629	1.5018	1.4176	1.4551	1.4960
d(C$_1$-O$_1$)	1.3438	1.3180	1.2559	1.3377	1.3084	1.2478
d(C$_2$-O$_2$)	1.3437	1.2768	1.2559	1.3376	1.2780	1.2478
d(O$_1$-H$_1$)	1.0253	1.1254	1.7664	1.0308	1.1737	1.7681
d(O$_2$-H$_2$)	1.0251	1.5345	1.7663	1.0291	1.4132	1.7686
d(O$_A$-H$_1$)	1.5328	1.2937	0.9853	1.4881	1.2064	0.9795
d(O$_B$-H$_2$)	1.5338	1.0178	0.9853	1.4945	1.0466	0.9795
d(O$_A$-O$_B$)	1.3262	1.3883	1.4554	1.3040	1.3577	1.4264
<(O$_1$-C$_1$-C$_2$)	124.0	121.1	121.8	123.2	120.6	121.4
< (H$_1$-O$_1$-C$_1$)	117.3	112.9	132.1	116.7	108.2	131.8
< (O$_1$-H$_1$-O$_A$)	172.7	179.6	173.1	174.1	174.8	170.2
< (O$_2$-C$_2$-C$_1$)	124.0	122.5	121.8	123.2	122.3	121.4
< (H$_2$-O$_2$-C$_2$)	117.3	123.9	132.1	116.7	120.1	131.7
< (O$_2$-H$_2$-O$_B$)	172.6	174.0	173.1	173.5	172.5	170.1
< (C$_2$-C$_1$-O$_1$-H$_1$)	29.6	48.4	11.4	34.9	55.2	14.5
< (C$_1$-C$_2$-O$_2$-H$_2$)	29.1	23.8	11.4	33.1	30.9	14.4

S5. Transmission coefficients and rate constants obtained from fitted Eckart potentials

In this section we present details calculations of the transmission coefficients and rate constants obtained from fitted Eckart potentials. Transmission coefficients were calculated using the analytical solution for an asymmetric Eckart potential of the form

$$V = \frac{AY}{1+Y} + \frac{BY}{\left(1+Y\right)^2} + ZPE_{\mathrm{PRC}} \qquad \text{(S17)}$$

where $A = E_1 - E_{-1}$, $B = \left(\sqrt{E_1} + \sqrt{E_{-1}}\right)^2$. ZPE_{PRC} is the zero-point energy of the pre-reactive complex and $Y = \exp\left(\frac{2\pi(s-s_0)}{l}\right)$ where s is the reaction coordinate, s_0 the location of the maximum of the adiabatic potential energy function and l is the width of the barrier. E_1 and E_{-1} are the activation energies of the forward and reverse reactions ($E_1 = E_{\mathrm{TS}} + ZPE_{\mathrm{TS}} - E_{\mathrm{PRC}} - ZPE_{\mathrm{PC}}$; $E_{-1} = E_{\mathrm{TS}} + ZPE_{\mathrm{TS}} - E_{\mathrm{PC}} - ZPE_{\mathrm{TS}}$).

These calculations were performed using the CCSD(T)//B3LYP and CCSD(T)//M06-2X electronic energies with zero-point energy corrections in vacuum and in water, employing the ChemRate program[23]. In ChemRate the Eckart transmission coefficient κ is calculated using the equation

$$\kappa(T) = \int_{-V_{a(s=0)}}^{\infty} P'(E)\exp\left(-\beta E\right)\mathrm{d}E \qquad \text{(S18)}$$

where, $\beta = (k_B T)^{-1}$ and P'(E) is the first derivate of the tunneling transition probability P(E) at total energy E, which is calculated using the analytical formula of Eckart[24]

$$P(E) = 1 - \frac{\cosh\left[2\pi\left(\alpha_1 - \alpha_2\right)\right] + \cosh\left[2\pi\delta\right]}{\cosh\left[2\pi\left(\alpha_1 + \alpha_2\right)\right] + \cosh\left[2\pi\delta\right]} \qquad \text{(S19)}$$

here, $\alpha_1 = \frac{1}{2}\left(\frac{E}{C}\right)^{1/2}$; $\alpha_2 = \frac{1}{2}\left[\frac{E-A}{C}\right]^{1/2}$; $\delta = \frac{1}{2}\left[\frac{B-C}{C}\right]^{1/2}$

$C = (h/2l)^2 \cdot (2\mathrm{m})^{-1}$ where h is the Planck's constant, m the mass of the particle (assumed as constant and equal to 1 amu) and l is the width of the barrier (see above). A, B, and l were calculated fitting the asymmetric adiabatic Eckart potential to the adiabatic ground-state potential energy (V_{AG}) profile obtained with the intrinsic reaction coordinate (IRC) method.[25] The results of the adiabatic ground-state potential energy are depicted in Figure S7.

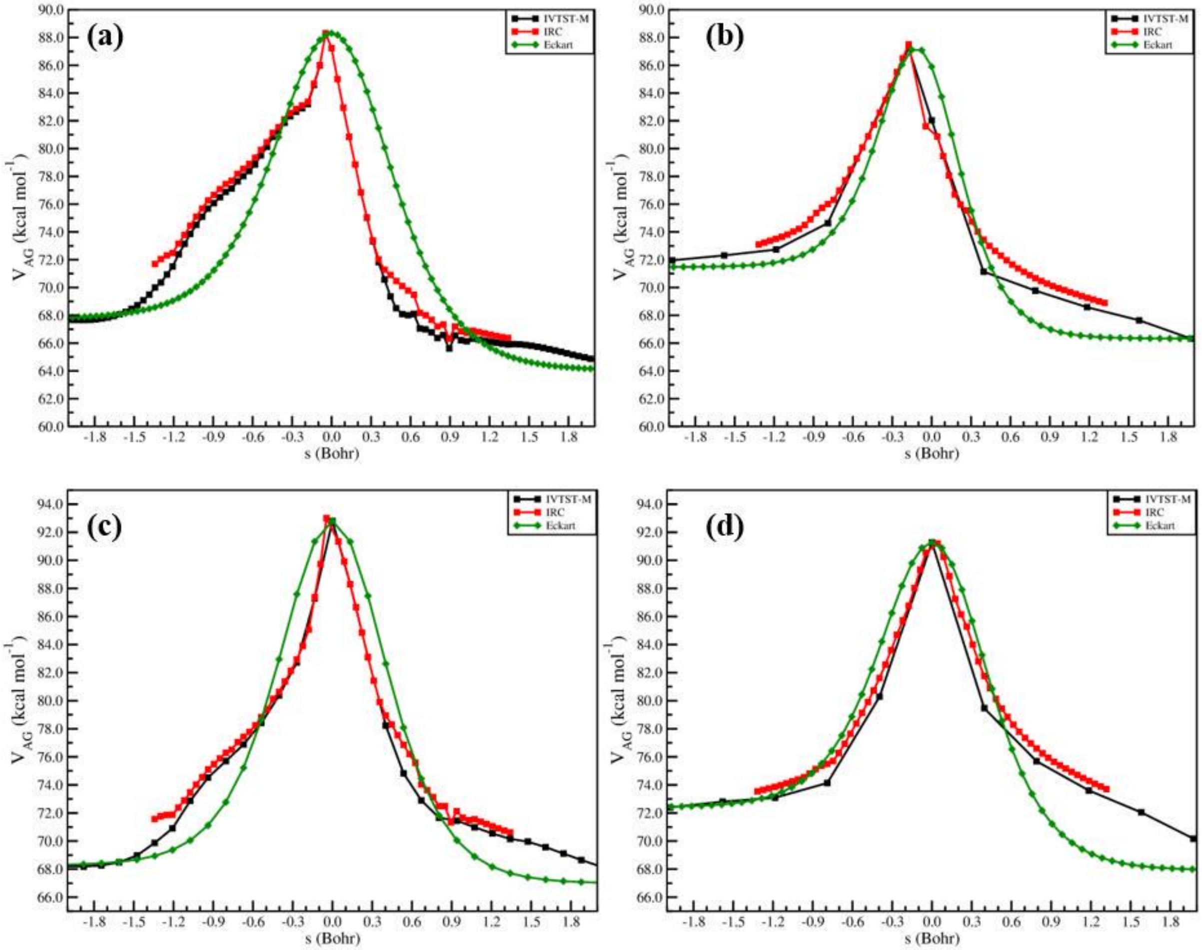

Figure S7. Adiabatic ground-state potential energy (V_{AG}) profiles, obtained with the intrinsic reaction coordinate (IRC),[25] interpolated variational transition-state theory by mapping (IVTST-M)[26] and asymmetric Eckart potential, of the concerted double-proton-transfer electron-transfer reaction between catechol and $O_2^{\bullet -}$. (a) CCSD(T)//B3LYP in water, (b) CCSD(T)//M062X in water, (c) CCSD(T)//B3LYP in vacuum, (d) CCSD(T)//M062X in vacuum. Solvation model = SMD.

Rate constants and transmission coefficients (with SCT and Eckart treatments) are presented in Table S5.

Table S5. Rate constants (M^{-1} s^{-1}) and transmission coefficients for the concerted double proton-transfer electron-transfer reaction between catechol and $O_2^{\bullet -}$ in water and vacuum. CVT = canonical variational transition state theory. SCT = small curvature tunneling approximation. κ(Eckart): Eckart transmission coefficient. κ(SCT): SCT transmission coefficient. T = 298.15 K. Solvation model: SMD.

	CCSD(T) //B3LYP	CCSD(T) //M06-2X
	Water	
K_{eq}	1.38×10^{1}	7.55×10^{0}
k_2(CVT)	2.82×10^{-3}	2.03×10^{-1}
κ(SCT)	3.97×10^{6}	1.14×10^{8}
κ(Eckart)	5.22×10^{5}	7.32×10^{7}
$k_{\text{overall}} = K_{eq} \cdot k_2(\text{CVT}) \cdot \kappa(\text{SCT})$	1.54×10^{5}	1.74×10^{8}
$k_{\text{overall}} = K_{eq} \cdot k_2(\text{CVT}) \cdot \kappa(\text{Eckart})$	2.03×10^{4}	1.12×10^{8}
	Vacuum	
k_2(CVT)	1.74×10^{-6}	6.49×10^{-4}
κ(SCT)	8.56×10^{8}	7.27×10^{9}
κ(Eckart)	3.86×10^{9}	4.88×10^{7}
$k_{\text{overall}} = k_2(\text{CVT}) \cdot \kappa(\text{SCT})$	1.49×10^{3}	4.71×10^{6}
$k_{\text{overall}} = k_2(\text{CVT}) \cdot \kappa(\text{Eckart})$	6.71×10^{3}	3.16×10^{4}

As can be seen in table S5, using the fitted Eckart potentials we obtain similar transmission coefficients (differences of less than one order of magnitude) as with the SCT method in water. Also, the total rate constants are similar. In vacuum we obtain transmission coefficients with the Eckart potential, which are roughly similar to the ones obtained with the SCT method (one order of magnitude larger for the B3LYP optimized structures, two orders of magnitude smaller for the M06-2X optimized structures). Note however that the fit of the Eckart potential in case of the B3LYP optimized structures is not very good, due to the asymmetric shape of the energy barrier (see Figure S7).

S6. References

1 E. Lee-Ruff, A. B. P. Lever and J. Rigaudy, The reaction of catechol and derivatives with potassium superoxide, *Can. J. Chem.*, 1976, **54**, 1837–1839.

2 D. T. Sawyer, T. S. Calderwood, C. L. Johlman and C. L. Wilkins, Oxidation by superoxide ion of catechols, ascorbic acid, dihydrophenazine, and reduced flavins to their respective anion radicals. A common mechanism via a combined proton-hydrogen atom transfer, *J. Org. Chem.*, 1985, **50**, 1409–1412.

3 T. Nakayama and B. Uno, Quinone–Hydroquinone π-Conjugated Redox Reaction Involving Proton-coupled Electron Transfer Plays an Important Role in Scavenging Superoxide by Polyphenolic Antioxidants, *Chem. Lett.*, 2010, **39**, 162–164.

4 S. V. Jovanovic, S. Steenken, M. Tosic, B. Marjanovic and M. G. Simic, Flavonoids as Antioxidants, *J. Am. Chem. Soc.*, 1994, **116**, 4846–4851.

5 D. J. Deeble, B. J. Parsons, G. O. Phillips, H.-P. Schuchmann and C. Von Sonntag, Superoxide Radical Reactions in Aqueous Solutions of Pyrogallol and N-propyl Gallate: The Involvement of Phenoxyl Radicals. A Pulse Radiolysis Study, *Int. J. Radiat. Biol.*, 1988, **54**, 179–193.

6 A. V. Marenich, C. J. Cramer and D. G. Truhlar, Universal Solvation Model Based on Solute Electron Density and on a Continuum Model of the Solvent Defined by the Bulk Dielectric Constant and Atomic Surface Tensions, *J. Phys. Chem. B*, 2009, **113**, 6378–6396.

7 W. Caminati, S. Di Bernardo, L. Schäfer, S. Q. Kulp-Newton and K. Siam, Investigation of the molecular structure of catechol by combined microwave spectroscopy and AB initio calculations, *J. Mol. Struct.*, 1990, **240**, 263–274.

8 H. Wunderlich and D. Mootz, Die Kristallstruktur von Brenzcatechin: eine Neubestimmung, *Acta Crystallogr. Sect. B Struct. Crystallogr. Cryst. Chem.*, 1971, **27**, 1684–1686.

9 R. L. Redington, W. B. Olson and P. C. Cross, Studies of Hydrogen Peroxide: The Infrared Spectrum and the Internal Rotation Problem, *J. Chem. Phys.*

10 K. G. Lubic, T. Amano, H. Uehara, K. Kawaguchi and E. Hirota, The ν1 band of the DO2 radical by difference frequency laser and diode laser spectroscopy: The equilibrium structure of the hydroperoxyl radical, *J. Chem. Phys.*

11 J. J. Warren, T. A. Tronic and J. M. Mayer, Thermochemistry of Proton-Coupled Electron Transfer Reagents and its Implications, *Chem. Rev.*, 2010, **110**, 6961–7001.

12 L. He, D. E. Fullenkamp, J. G. Rivera and P. B. Messersmith, pH responsive self-healing

hydrogels formed by boronate–catechol complexation, *Chem. Commun.*, 2011, **47**, 7497.

13 S. Steenken and P. Neta, Electron transfer rates and equilibriums between substituted phenoxide ions and phenoxyl radicals, *J. Phys. Chem.*, 1979, **83**, 1134–1137.

14 H. Yin, Q. Zhang, Y. Zhou, Q. Ma, T. Liu, L. Zhu and S. Ai, Electrochemical behavior of catechol, resorcinol and hydroquinone at graphene–chitosan composite film modified glassy carbon electrode and their simultaneous determination in water samples, *Electrochim. Acta*, 2011, **56**, 2748–2753.

15 J. Kennedy, M. Munro, H. Powell, L. Porter and L. Foo, The protonation reactions of catechin, epicatechin and related compounds, *Aust. J. Chem.*, 1984, **37**, 885.

16 S. Suresh, V. C. Srivastava and I. M. Mishra, Adsorption of catechol, resorcinol, hydroquinone, and their derivatives: a review, *Int. J. Energy Environ. Eng.*, 2012, **3**, 32.

17 G. Ivanova, E. Bratovanova and D. Petkov, Catechol as a nucleophilic catalyst of peptide bond formation, *J. Pept. Sci.*, 2002, **8**, 8–12.

18 D. T. Sawyer and J. S. Valentine, How super is superoxide?, *Acc. Chem. Res.*, 1981, **14**, 393–400.

19 D. T. Sawyer and M. J. Gibian, The chemistry of superoxide ion, *Tetrahedron*, 1979, **35**, 1471–1481.

20 D. R. Lide, *CRC Handbook of Chemistry and Physics, 90th Edition (CRC Handbook of Chemistry & Physics)*, 2009.

21 A. A. N.-C. R. V. N. C. Maroziene, Correlation between mammalian cell cytotoxicity of flavonoids and the redox potential of phenoxyl radical/phenol couple, *Acta Biochim. Pol.*, 2012, **59**, 299–306.

22 G. Buettner, The Pecking Order of Free Radicals and Antioxidants: Lipid Peroxidation, α-Tocopherol, and Ascorbate, *Arch. Biochem. Biophys.*, 1993, **300**, 535–543.

23 V. Mokrushin, V. Bedanov, W. Tsang, M. Zachariah, R., V. Knyazev, D. and W. Sean McGivern, ChemRate: A tool for RRKM/Master Equation Modeling. http://kinetics.nist.gov/ChemRate.

24 C. Eckart, The Penetration of a Potential Barrier by Electrons, *Phys. Rev.*, 1930, **35**, 1303–1309.

25 C. Gonzalez and H. B. Schlegel, Reaction path following in mass-weighted internal coordinates, *J. Phys. Chem.*, 1990, **94**, 5523–5527.

26 J. C. Corchado, E. L. Coitiño, Y.-Y. Chuang, P. L. Fast and D. G. Truhlar, Interpolated Variational Transition-State Theory by Mapping, *J. Phys. Chem. A*, 1998, **102**, 2424–2438.